Computational Materials Science 154 (2018) 204–211

Contents lists available at ScienceDirect

Computational Materials Science

journal homepage: www.elsevier.com/locate/commatsci

Two-dimensional sheet of germanium selenide as an anode material for sodium and potassium ion batteries: First-principles simulation study

Arindam Sannyal[a], Zhengqing Zhang[a], Xingfa Gao[b,*], Joonkyung Jang[a,*]

[a] Department of Nanoenergy Engineering, Pusan National University, Busan 46241, Republic of Korea
[b] College of Chemistry and Chemical Engineering, Jiangxi Normal University, Nanchang 330022, China

ARTICLE INFO

Keywords:
Density functional theory
2D materials
Germanium selenide
Anisotropic diffusion
Capacity
Na-ion battery
K-ion battery

ABSTRACT

Recently, two-dimensional layered materials have come forth as encouraging candidates for advanced electronic and optoelectronic applications. Anode materials with high energy-density and diffusion rate are fundamental features for the development of non-lithium ion batteries. Based on the density functional theory calculations, we propose a two-dimensional (2D) sheet of germanium selenide (GeSe) as a promising anode material for a sodium (Na) or potassium (K) ion battery. The phonon dispersion and formation energy verify the dynamic and thermal stability of the GeSe sheet. A substantial charge transfer from the alkali metal atoms to the GeSe sheet enhances the electrical conductivity of GeSe, favorable for an anode material. The Na or K diffusion on the GeSe sheet has a low energy barrier of 0.10 eV, giving a rapid charge/discharge rate without metal clustering. The GeSe sheet has a high theoretical capacity for both Na (707 mA h g^{-1}) and K (530 mA h g^{-1}) ion batteries. The GeSe sheet also gives a low and stable electrode potential comparable to that of a commercial anode material.

1. Introduction

The high cost of lithium (Li) limits the applications of lithium-ion batteries (LIBs) for large-scale energy systems, such as smart grids, stationary power stations, and fully electric vehicles [1]. Consequently, sodium (Na) and potassium (K) ion batteries (NIBs and KIBs) have attracted considerable interest because of the higher abundances of Na and K and the similar storage mechanisms of NIBs and KIBs to those of LIBs [2–7]. A successful commercialization of NIB or KIB is limited by, among others, the lack of a suitable anode material [8,9] with a rapid charge/discharge rate, a high storage capacity, and a good capacity retention.

In this regard, two-dimensional (2D) materials, having high surface areas and superior electronic properties [10], are considered as anode materials of LIBs, NIBs, and KIBs [11–16]. For example, a 2D black phosphorus, phosphorene, gives a high storage capacity in NIB [17–19], but it is thermally unstable and highly reactive towards O_2 and H_2O [20–22]. Graphene contact or hexagonal boron nitride (h-BN) encapsulation of phosphorene [23,24] were proposed as strategies to prevent the oxidative degradation. In contrast, 2D materials of group-IV monochalcogenides MX (M = Si, Ge or Sn; X = S or Se) are known for their stability, abundance, and environmental friendliness [25–29]. By comprehensive first-principle calculations Zhou et al. showed that, compared to phosphorene, the monolayers of group-IV monochalcogenides have enhanced oxidation resistivities and thermodynamic stabilities under ambient conditions [29]. A theoretical study showed a 2D GeS sample has nice features of the theoretical capacity and charging rate for NIB application [21]. Among monochalcogenides, the 2D sheet of GeSe has a direct band gap [26]. Multi-layered sheets of GeSe are recently applied to photovoltaic and photodetector applications [30–32]. An anode material made from GeSe nanocrystals shows an excellent capacity retention for LIB [33]. Kim et al. reported that a comb-shaped GeSe has high rate capability (331 mA h g^{-1} at 20 C) and remarkable cyclability (650 mA h g^{-1} even after 1000 cycles) when used in a LIB [34]. In addition, first-principle study showed that a 2D sheet of GeSe can be a good candidate for LIBs [35].

However, currently, the applicability of a 2D GeSe sheet for a NIB or KIB is unknown. Herein, the density functional theory (DFT) simulations are performed to provide a comprehensive understanding on the prospective application of a single-layered GeSe sheet for NIB or KIB. The thermal and dynamic stabilities of the GeSe sheet and the practicality of its isolation from the bulk GeSe are confirmed. The Na or K diffusion on the GeSe sheet has a low energy barrier of 0.1 eV. Moreover, the 2D GeSe sheet gives high theoretical capacities and low and stable voltages for NIB and KIB. All these results indicate that a GeSe sheet is a prospective anode material which gives a high-power density and a rapid charge/discharge rate.

* Corresponding authors.
E-mail addresses: gaox@jxnu.edu.cn (X. Gao), jkjang@pusan.ac.kr (J. Jang).

https://doi.org/10.1016/j.commatsci.2018.08.002
Received 4 May 2018; Received in revised form 30 July 2018; Accepted 1 August 2018
Available online 06 August 2018
0927-0256/

2. Computational details

All the DFT calculations are performed using the Vienna ab initio simulation package (VASP) [36,37]. The electron-ion interactions are considered using the projector-augmented wave method [38]. We treat the exchange correlation within the generalized gradient approximation in the form of the Perdew–Burke–Ernzerhof [39] functional. We use an energy cutoff of 500 eV in the plane-wave expansion of a valence electron wave function. The van der Waals interactions are included using the semiempirical correction scheme of Grimme (DFT + D2) [40] which successfully describes the binding energy and diffusion of lithium on graphite [41]. To examine the adsorption and diffusion of metal atoms, we model the 2D GeSe sheet as a 3 × 3 slab, repeated periodically along the X and Y directions. A 20 Å-thick vacuum space is introduced along the Z-direction to avoid the spurious interactions between the GeSe sheet and its periodic images. We optimize both the lattice constants and atomic coordinates using the conjugate gradient scheme without imposing any symmetry restrictions. A geometry optimization is taken to be converged if the change in energy is $< 10^{-5}$ eV and the maximum force on each atom is < 0.02 eV Å^{-1}.

We check the dynamic stability of the GeSe sheet by calculating its phonon dispersion spectra using the Phonopy code [42]. The Brillouin zones of the 2D and bulk GeSe are sampled using 4 × 4 × 1 and 4 × 3 × 4 Monkhorst-Pack [43] k-point grids, respectively. We use a denser mesh of 12 × 12 × 1 to calculate the DOS and band structure of the GeSe sheet. We employ the Bader charge analysis [44–46] to determine the amount of charge transfer between metal and GeSe. We study the diffusion of alkali metal atom by constructing the minimum energy path based on the climbing image nudged elastic band (CI-NEB) method implemented in the VASP transition state tools [47,48]. Nine images are used, including the initial and final configurations in the CI-NEB calculation. The zero-point energy (ZPE) and quantum tunneling effects on the present ionic diffusion are expected to be small, as found for Li diffusions on 2D SiS and SiSe [49] and Na diffusions in hexagonal boron nitride/black phosphorene heterostructure [50].

3. Results and discussions

3.1. Structure of GeSe nanosheet

Our calculation gives the lattice parameters of the bulk GeSe as a = 3.87 Å, b = 4.53 Å, and c = 11.142 Å, which are consistent with the previous theoretical studies using PW91 and PBE functional [25,27]. The maximum deviations are within 3%. The 2D GeSe sheet shows a puckered layer structure [51] (as shown in Fig. 1). The calculated lattice parameters are a = 3.94 Å and b = 4.42 Å. The lattice parameters agree with previous computation using PBE functional (deviation < 1%) [26]. The 2D GeSe have two distinct Ge–Se bond lengths, l_1 = 2.61 Å and l_2 = 2.54 Å (Fig. 1a).

The thickness of the GeSe d (=2.52 Å) is greater than that of phosphorene (=2.10 Å) (Fig. 1a). We estimate the thermodynamic stability of the GeSe sheet by calculating the formation energy E_f defined as

$$E_f = E_{GeSe} - E_{Ge} - E_{Se} \quad (1)$$

where E_{GeSe} is the energy of the GeSe sheet and E_{Ge} and E_{Se} are the energies of Ge and Se atoms in the bulk, respectively. E_f is found to be −0.25 eV per unit cell, confirming that the GeSe sheet is thermodynamically stable (ignoring the entropic contribution which is negligible at room temperature) [52,53].

We assess the dynamic stability of the GeSe sheet by examining the phonon dispersion calculated using the density functional perturbation theory [54]. The phonon spectra do not exhibit any imaginary frequency (Fig. S1), proving the vibrational stability of the GeSe sheet. Twelve modes of vibrations are present: three acoustic (lower curves) and nine optical modes (upper curves). The optical and acoustic branches are well separated, as found for other 2D materials, such as graphene [55], phosphorene [56], and stanene [57]. We evaluate the exfoliation energy of the GeSe sheet, E_{exf}, as

$$E_{exf} = \left(\frac{E_{bulk}}{N} - E_{mono}\right) \quad (2)$$

where E_{bulk} and E_{mono} are the energies of the bulk GeSe made from N (=2) layers per unit cell and the GeSe sheet, respectively. Compared to the traditional few-layer slab model, the present method gives exfoliation energies with less computation time and reasonable accuracy [15,58,59]. We find E_{exf} = 0.14 eV per unit cell, comparable to those of the experimentally synthesized graphene (0.21 eV), boron nitride (0.28 eV) [59], MoN_2 (0.17 eV) [15], and MoS_2 (0.16 eV) [15,58]. Therefore, a common method such as mechanical exfoliation [60,61] and liquid exfoliation [62,63] can be used to grow the GeSe sheet.

3.2. Adsorption of alkali metal atoms on GeSe nanosheet

We examine how strongly the GeSe sheet binds the alkali metal atoms. A weak binding of metal can give an undesirable metal

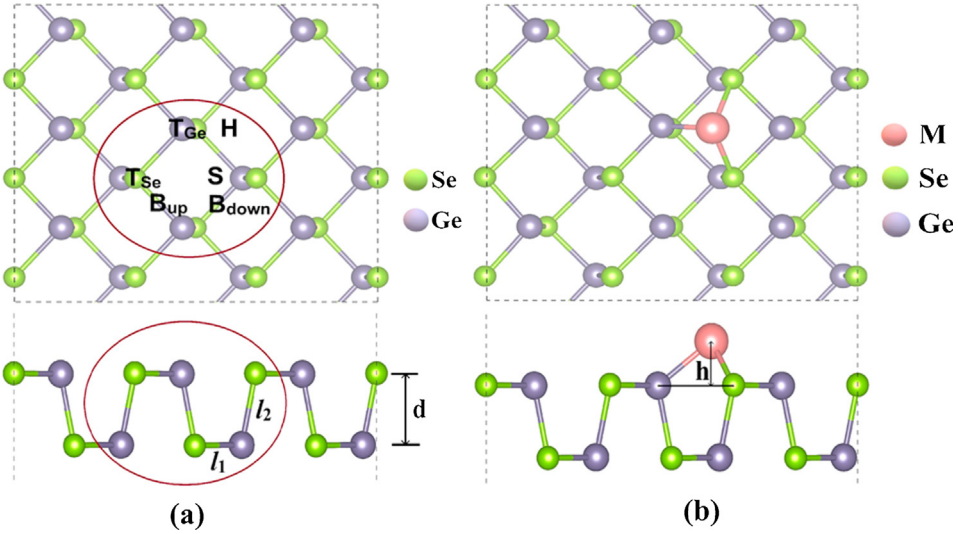

Fig. 1. (a) Adsorption sites on the 2D GeSe sheet labelled with different letters (H, S, T, and B). The circles denote the unit cells. (b) An alkali metal atom (Li in this case) adsorbed at site H which gives the strongest metal adsorption. In each panel, the top and side views are shown together.

Table 1
Binding energies of alkali metal atoms E_{bind} s (in eV) adsorbed at six different sites of the GeSe sheet (Fig. 1a). Also listed are the heights of the alkali metal atoms and the metal-to-GeSe charge transfer $\Delta\rho$ calculated from the Bader analysis. Both h and $\Delta\rho$ are calculated for metal atoms adsorbed at H sites (Fig. 1b).

	E_{bind}^{H}	E_{bind}^{S}	$E_{bind}^{B_{down}}$	$E_{bind}^{B_{up}}$	$E_{bind}^{T_{Se}}$	$E_{bind}^{T_{Ge}}$	h^H (Å)	$\Delta\rho^H$ (IeI)
Li	−1.92	−1.84	−1.61	−1.30	−1.04	−0.88	1.39	0.79
Na	−1.25	−1.23	−1.11	−0.90	−0.86	−0.79	2.12	0.60
K	−1.36	−1.32	−1.21	−1.01	−0.99	−0.96	2.52	0.74

clustering (as found for pure graphene) which limits the performance of the graphene sheet for a battery application [49,64,65]. As shown in Fig. 1a, we first consider a single metal atom adsorbed at one of six sites on the GeSe sheet, i.e., above the center of the triangle ring consisting of two Ge atoms and one Se atom (H site) and two Se atoms and one Ge atom (S site), top of a upper Ge–Se bond (B_{up} site) and lower Ge–Se bond (B_{down} site), and top of an upper Se atom (T_{Se} site) and a Ge atom (T_{Ge} site). For a given metal M, we define the binding energy, E_{bind}, as

$$E_{bind} = (E_{MGeSe} - E_{GeSe} - N \times E_M)/N \quad (3)$$

where E_{MGeSe}, E_{GeSe}, and E_M are the energies of the GeSe sheet adsorbed with N metal atoms, the pristine GeSe sheet, and the isolated metal atom, respectively. Table 1 lists E_{bind} for various adsorption sites. The metal binding at H site is the strongest because of its high coordination number [21,66,67]. The E_{bind}s of Li, Na, and K atoms at H sites are −1.92, −1.225, and −1.326 eV, respectively, which are stronger than the cohesive energies of metal atoms (Li = −1.63, Na = −1.13, and K = −0.94 eV) [68]. We investigate the energy vs. the height (h) of the metal atom at site H (Fig. 1b). This energy decreases steeply from zero to the minimum with decreasing h below 6 Å (Fig. S2). No energy barrier exists in this surface loading process. The h at the minimum (1.39, 2.12, and 2.52 Å for Li, Na, and K, respectively) increases with increasing atomic number. With further decreasing the height from the minimum point, the energy sharply increases.

To have further insight into the adsorption process, we calculate the charge density difference $\Delta\rho$ between GeSe and metal atom as

$$\Delta\rho = \rho_{MGeSe} - \rho_{GeSe} - \rho_M \quad (4)$$

where ρ_{MGeSe}, ρ_{GeSe}, and ρ_M are the charge densities of the metal-adsorbed and the pristine GeSe sheets, and isolated metal atom, respectively. Fig. 2 presents the charge dispersions of Li, Na, and K atoms adsorbed at H sites. Clearly, a substantial electronic charge transfers from the metal atom to the three adjacent atoms of the GeSe sheet (two Se atoms and one Ge atom). The Bader charge analysis gives charge transfers of 0.79e, 0.60e and 0.74e for Li, Na, and K atoms, respectively.

On the other hand, using the ultrasoft pseudopotential (US-PP), S. Karmakar et al. [49] reported that Li donates 0.99e to the 2D GeSe. This difference likely arises from the use of different potentials (US-PP vs PAW method). A similar discrepancy is found for Li adsorption on 2D GeS as well [21]. The alkali metal atoms essentially exist in their cationic states and the metal atoms are chemically adsorbed on the GeSe sheet. This is compatible with the fact of greater electronegativity of Ge and Se compared to the alkali metal atoms. The charge transfer from metal to GeSe increases with strengthening the metal-GeSe binding (decreasing E_{bind}). This trend is reasonable because the metal-to-surface charge transfer is known to be responsible for the strong adsorption of the metal atoms [19,69]. We investigate the electronic density of states (DOS) and band structure of the GeSe sheet upon metal adsorption. For pristine GeSe sheet, we observe a direct gap of 1.34 eV between the valence band maximum (VBM) and conduction band minimum (CBM) (Fig. S3a), which is consistent with other calculated values [26,70]. Fig. 3 shows the total DOS (TDOS) and partial DOS (PDOS). The PDOSs show that Se 4p and Ge 4p orbitals mainly contribute to the VBM and

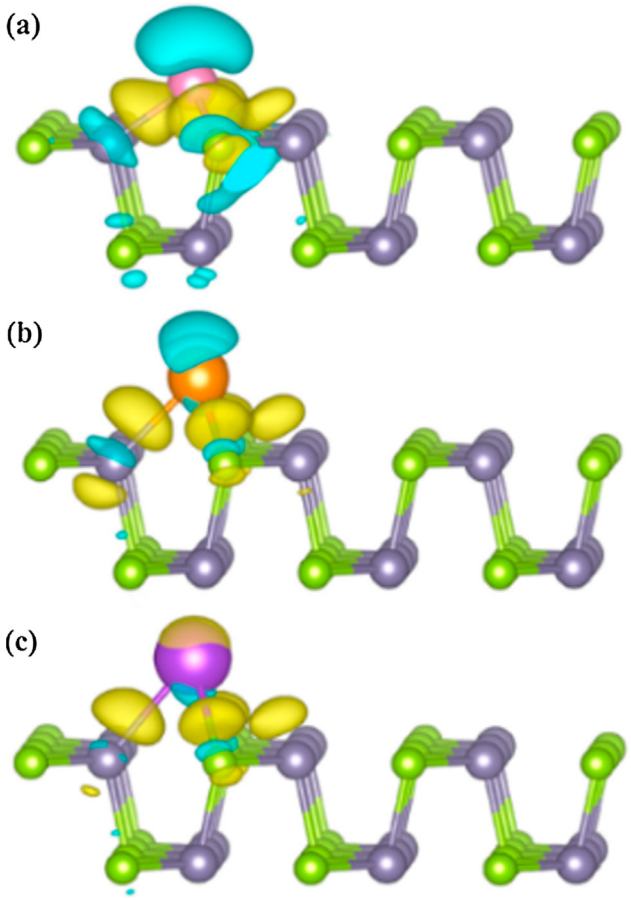

Fig. 2. Differential charge densities of the GeSe sheets adsorbed with a Li (a), Na (b), and K (c) atom. The electron depletion and accumulation, respectively, are drawn in cyan and yellow colors. The isovalue is taken to be 0.002 IeI bohr^{-3}.

CBM, respectively. The significant charge transfer from metal to GeSe effectively shifts the Fermi energy level into the conduction band resulting enhanced electrical conductivity of the 2D GeSe. At the lowest concentration of metal ($M_{0.05}$GeSe), one band crosses the Fermi level (Fig. S3). As the Fermi level has not shifted deep into the conduction band, the 2D GeSe adsorbed with a single metal atom is rather n-doped semiconducting than metallic. The previous studies showed however that with increasing concentration of Na atoms, the band gap of Na-phosphorene complex gradually decreases and eventually disappears [18,19]. A full lithiation of 2D SiS/SiSe showed a similar behavior [49]. Therefore, with increasing metal atom concentrations, the present 2D GeSe will become metallic.

3.3. Diffusion of alkali metal atoms on GeSe nanosheet

A facile diffusion of metal atom on the GeSe sheet will give a rapid charge-discharge rate [71] for an anode made of this material [72]. We find that a metal atom diffuses on the GeSe sheet via two distinct pathways: one along the zigzag direction (H_0-B_1-S_1-B_2-H_1) and the other along the armchair direction (H_0-T_1-H_2), as shown in Fig. 4a–c. The energy profiles for the diffusions along the zigzag and the armchair directions are plotted in Fig. 4d and e, respectively. Upon moving from H_0 to H_1 site along the zigzag direction, a metal atom encounters two energy barriers (B_1 and B_2) of equal heights and a metastable site (S_1) located at a local energy minimum. The energy barriers of Li, Na, and K atoms along this pathway are 0.291, 0.115, and 0.11 eV, respectively. The energy barrier of the Li diffusion is larger than those of Na and K because the Li atom adsorbs more strongly than the Na and K atoms do.

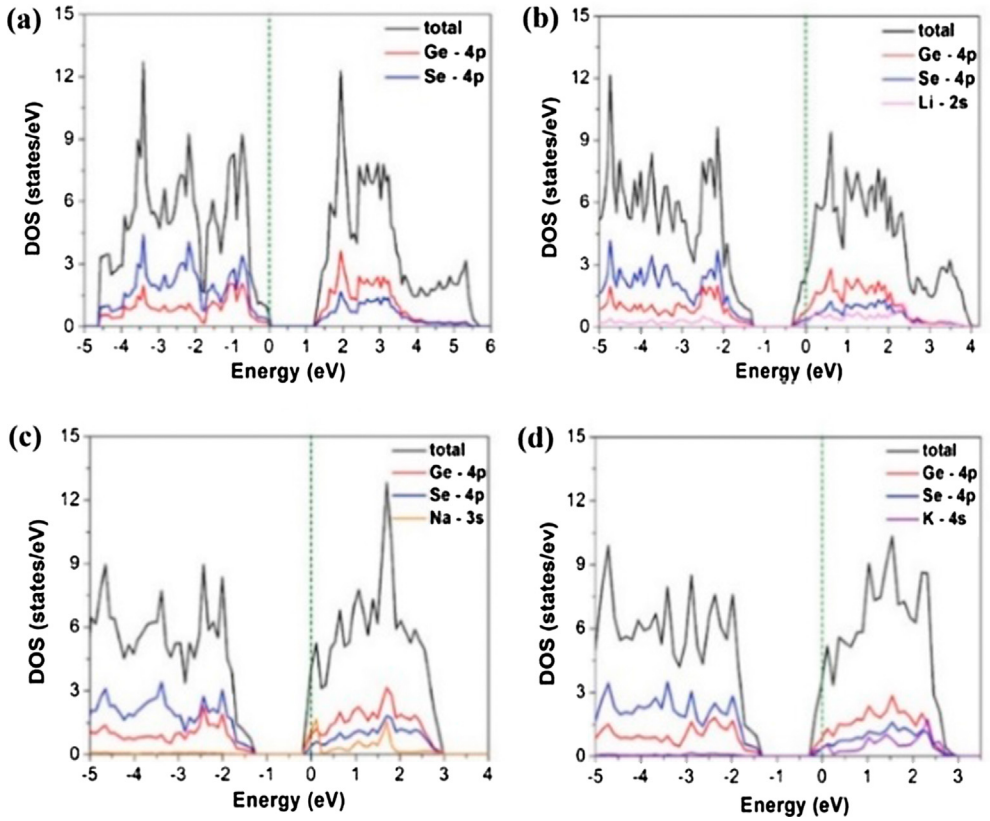

Fig. 3. Total and partial DOSs for 2D structures of the pristine GeSe (a), $Li_{0.05}GeSe$ (b), $Na_{0.05}GeSe$ (c) and $K_{0.05}GeSe$ (d). The PDOSs of the metal ions are enlarged tenfold for visibility. The Fermi level is set to zero energy.

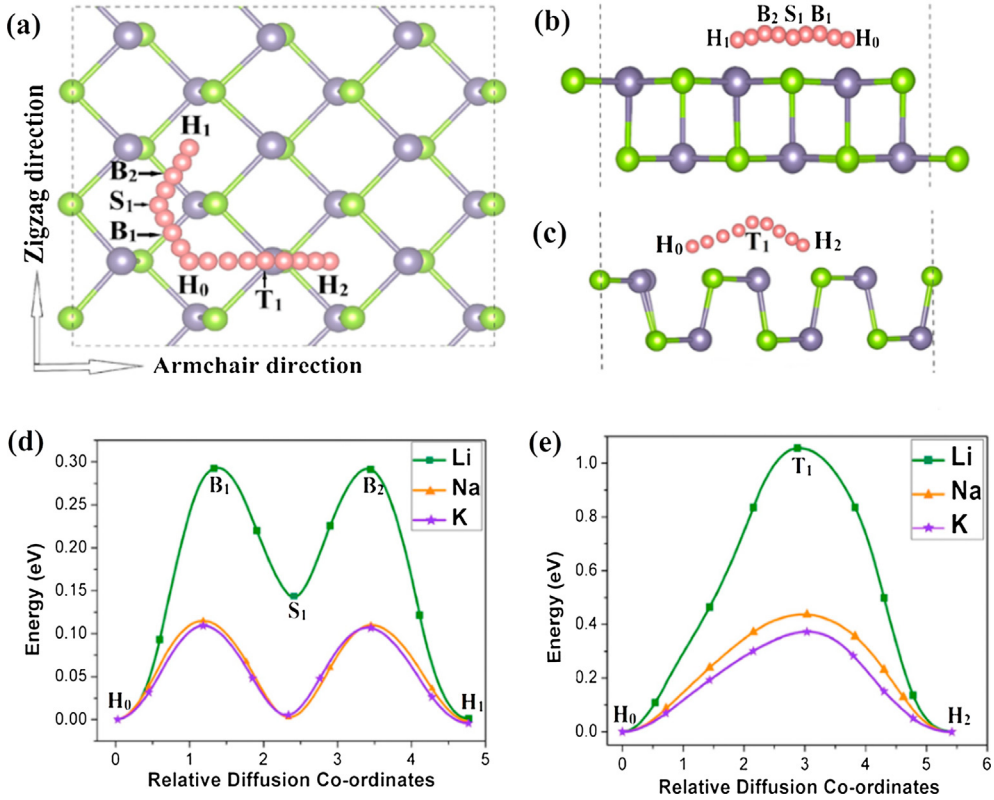

Fig. 4. Diffusion pathways of alkali metal atoms on the GeSe sheet. Top (a) and side (b and c) views are drawn together. Minimum energy profiles of alkali metal atoms diffusing along the (d) zigzag and (e) armchair directions.

These diffusion barriers are much lower than those found for boron phosphide (0.15–0.36 eV) [72], graphene (0.33 eV) [73], MoN_2 (0.49–0.78 eV) [15], Si (0.57 eV) [74,75], Sn (0.39 eV) [76], and TiO_2-based polymorphs (~0.65 eV) [77,78]. The diffusion barriers of the alkali metal atoms on different group-IV monochalcogenides and other 2D materials are listed in Table S1.

A metal atom diffusing along the armchair direction faces a single energy barrier located at T_1. Along with this direction, the energy barriers of Li, Na, and K diffusion are 1.056, 0.43, and 0.37 eV, respectively, which are higher than those along the zigzag pathway. This is because, along with the armchair direction, the metal atoms face strong ionic repulsion with the Ge atom at site T_1. Using the Arrhenius equation [17,79], the diffusion constant D is given by

$$D \approx \exp\left(-\frac{E_a}{k_B T}\right) \tag{5}$$

where E_a and k_B are the activation energy and Boltzmann constant, respectively. Accordingly, Li, Na, and K atoms diffuse along the zigzag direction 8.664×10^{12}, 2.124×10^5, and 2.5×10^4 times faster, respectively, than along the armchair direction (at room temperature). This high diffusion barrier effectively limits the metal atoms in the zigzag direction and thus presumably prevents the clustering of metal atoms [21,80], endowing the GeSe sheet with a long cycle life.

With increasing the atomic number, a metal atom grows in size and therefore is placed farther above the 2D GeSe surface (manifested in the enhanced *h*s). Consequently, the ionic repulsions between the nuclei of the metal atom and GeSe are reduced in the diffusion pathways. Therefore, the diffusion becomes faster with increasing the atomic number. With the increasing atomic number of metal, the energy barrier and directional anisotropy of diffusion decreases. Even for Na and K atoms, the difference between the barriers along two pathways are still very high (> 0.25 eV). Therefore, the diffusion along the armchair direction and the resulting formation of metal clusters are effectively blocked. The low diffusion barrier along zigzag direction makes monolayer GeSe a potential anode, especially for Na and K battery application. We also investigate metal atoms diffusing in the bulk GeSe ($3 \times 3 \times 2$) along the zigzag direction, as summarized in Fig. 5. The bulk GeSe structure was modeled with our calculated lattice parameters. The diffusions of Li and Na atoms exhibit two energy barriers separated by a local minimum in energy, which is similar to those found for the GeSe sheet. The diffusion of K atom has no metastable state, however, presumably because of the large atomic radius of K. The diffusion barriers of Li, Na, and K atoms are 0.42, 0.28, and 0.25 eV, respectively. The calculated energy barriers in the bulk GeSe are higher than those measured on the GeSe sheet, owing to the spatial hindrance arising from the interlayer interaction existing in the bulk GeSe [17]. Notably, the diffusivities of Na and K atoms in the bulk GeSe are still larger than that of Li in the bulk GeSe or on graphene (0.33 eV) [73].

3.4. Voltage profile and specific capacity

We examine the average adsorption energies E_{ave} s of metal atoms located in different layers of the GeSe sheet. The E_{ave} of the *nth* layer is given by

$$E_{ave} = \frac{E(M_{8n}GeSe) - E(M_{8(n-1)}GeSe) - 8E_M}{8} \tag{6}$$

where $E(M_{8n}GeSe)$ and $E(M_{8(n-1)}GeSe)$ are the energies of the GeSe sheets adsorbed with n and $n-1$ layers of metal atoms, respectively, and E_M is the energy per atom in the bulk metal. Note that both sides of the GeSe sheet are adsorbed and a total of eight atoms are adsorbed in each layer (four atoms on either side of GeSe in the present 2×2 supercell). E_{ave} indicates whether metal atoms bind to the *n*th layer ($E_{ave} < 0$) or cluster themselves ($E_{ave} > 0$). The E_{ave} of Li atoms in the first layer is −0.26 eV, but the Li atoms in the second layer are unstable (Fig. S4a). A similar behavior is reported in the adsorption of Li on a 2D GeS sheet [21]. For Na adsorption, the present GeSe sheet holds up to four adsorbed layers on each side. The E_{ave}s of the first, second, third, and fourth layers are −0.33, −0.20, −0.136, and −0.132 eV, respectively. The adsorption in the fifth layer of Na gives a negative E_{ave} (−0.152 eV), but causes a severe bond elongation (11.3%) between the Ge and Se atoms (l_2) (Fig. S4b). The structural instability of the 2D GeSe might be overcome by controlling the cut-off voltage to limit the AM concentration, as a commercial $LiCoO_2$ battery is operated under 4.2 V to prevent the instability at a higher voltage (4.5 V) [81]. Finally, the E_{ave}s of K atoms in the first, second, and third layer vary as −0.46, −0.036, and −0.032 eV, respectively. The E_{ave}s of the second and third layers of K atoms are relatively weak but still comparable to or even stronger than found for Li on Nb_2C (−0.02 eV per atom) [82] and Na on Ca_2N (−0.003 eV per atom) [83], MoN_2 (−0.02 eV per atom) [15], and GeS (−0.02 eV per atom) [21]. However, for the fourth layer of K atoms, the E_{ave} becomes positive (0.06 eV), indicating the formation of metal clusters in the fourth layer.

We investigate the open circuit voltage (OCV) and the storage capacity of the GeSe sheet. The following half-cell reaction (vs. M/M^+) is considered:

$$GeSe + x\ M^+ + x\ e^- \leftrightarrow M_x GeSe$$

The intercalation potential is calculated by considering only the thermodynamically stable phases. A piecewise voltage profile is obtained by constructing a formation energy convex hull. To calculate the DFT formation energy, all the symmetrically distinct configurations are generated by using Python Materials Genomics (Pymatgen) [84] package. The formation energy ΔE_{form}, is calculated as

$$\Delta E_{form} = E_{M_xGeSe} - E_{GeSe} - x \times E_{M_{bulk}} \tag{7}$$

where E_{M_xGeSe}, E_{GeSe}, and $E_{M_{bulk}}$ are the energies of the GeSe sheet adsorbed with x metal atoms, the pristine GeSe sheet, and the energy per metal atom in the bulk, respectively. Fig. 6(a) shows the formation

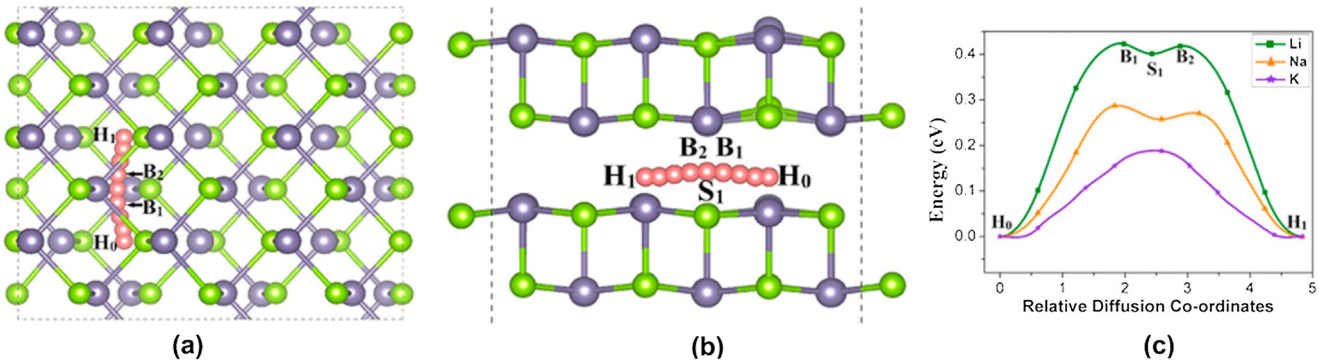

Fig. 5. Top (a) and side (b) views of Li atoms diffusing in the bulk GeSe. Energy profiles for the diffusions of metal atoms (c).

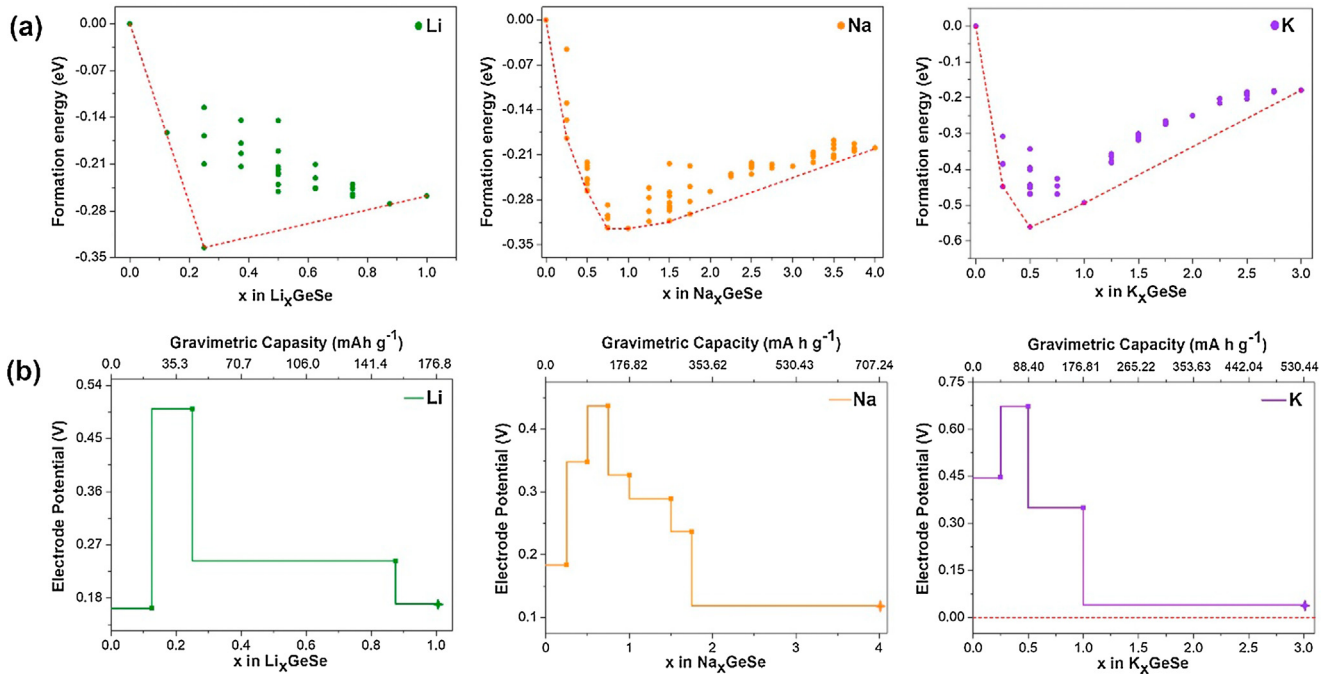

Fig. 6. (a) Calculated formation energy convex hull at different Li/Na/K concentrations and (b) voltage profile (vs M/M^+) using the concentration of the tie lines on the convex hull of Li_xGeSe, Na_xGeSe, and K_xGeSe systems. The stars indicate the maximum theoretical capacity for each alkali metal atom.

energy convex hull on which the intermediate phases are lying. The stable intermediate phases of M_xGeSe involve x s of 0.00, 0.125, 0.25, 0.875, and 1.00 for Li. Similarly, x values are 0.00, 0.25, 0.50, 0.75, 1.00, 1.50, 1.75, and 4.00 for Na and 0.00, 0.25, 0.50, 1.00, and 3.00 for K. These ionic concentrations are used to compute the electrode potential V [52,85] given by

$$V = -\frac{E(M_{x_2}GeSe) - E(M_{x_1}GeSe) - (x_2 - x_1)E_{M_{bulk}}}{(x_2 - x_1)e} \quad (8)$$

where $E(M_{x_2}GeSe)$ and $E(M_{x_1}GeSe)$ are the total energy of the GeSe sheet adsorbed with x_2 and x_1 metal atoms and $E_{M_{bulk}}$ is the energy per atom of the bulk metal. The voltage is related to the Gibbs free energy G ($= \Delta E + P\Delta V - T\Delta S$), but the volume ($P\Delta V \approx 10^{-5}$ eV) and entropic effects ($T\Delta S \approx 25$ meV) are negligible at room temperature [52]. The electrode potentials of the 2D Li_xGeSe are 0.16–0.50 V with an average of 0.26 V. Upon connecting to a high voltage cathode ~4 V (as the average voltages of $LiCoO_2$ and $LiMn_2O_4$ are around 4.1–4.2 V vs Li/Li^+) [21,85–87], this will give a desirable OCV of 3.84–3.50 V. The 2D Na_xGeSe and K_xGeSe have electrode potentials of 0.12–0.44 V (OCV, 3.88–3.56 V) and 0.04–0.67 V (OCV, 3.96–3.33 V), with averages of 0.27 V and 0.38 V, respectively. The previous experiments [33,34] showed, during the first discharge process of Li insertion, the GeSe nanoparticle undergoes irreversible decomposition into Ge and Li_2Se at ~1.0–1.3 V. These Ge nanoparticles have high Coulombic efficiency through the reversible insertion/extraction process ($Ge + xLi \rightarrow Li_xGe$). These irreversible and reversible reactions will not take place for the present monolayer of GeSe which has theoretical voltages of 0.16–0.50 V.

The 2D GeSe sheet holds a maximum of 2 Li, 8 Na, and 6 K atoms per unit cell (Fig. 6). The electrode potentials of the GeSe sheet have average values comparable to those of commercial anode materials such as graphite (0.10 V) [88] and TiO_2 (1.5 V) [89]. The present voltages do not fluctuate from their averages by more than 0.33 V. These low electrode potentials and stable voltage profiles suggest that the 2D GeSe sheet qualifies as an anode material for LIB, NIB, and KIB applications. The GeSe sheet holds up to 1 Li, 4 Na, and 3 K layers, giving the stoichiometries of LiGeSe, Na_4GeSe, and K_3GeSe, respectively (Fig. S5). The theoretical capacity C is given by

$$C = \frac{x_{max}F}{MW_{GeSe}} \quad (9)$$

where x_{max} is the maximum fraction of metal atoms in M_xGeSe, F is the Faraday constant (26.8 A h mol^{-1}), and MW_{GeSe} is the molecular weight of GeSe (151.57 g mol^{-1}). The storage capacities of the 2D GeSe anodes for Li, Na and K atoms are 176.78 mA h g^{-1}, 707.12 mA h g^{-1}, and 530.44 mA h g^{-1}, respectively. Note that the present theoretical capacities for Na and K are much larger than those of other 2D anode materials reported previously, such as MXenes (Na < 400 and K < 200 mA h g^{-1}) [12], Mo_2C (Na 262 mA h g^{-1} and K 65 mA h g^{-1}) [72], MoS_2 (Na 335 mA h g^{-1}) [90], VS_2 (Na 233 mA h g^{-1}) [91], GeS (Na 512 and K 256 mA h g^{-1}) [21], SiS (Na 445 mA h g^{-1}) [92], and graphite (K 279 mA h g^{-1}) [93]. The previous studies report that the Na storage capacity of the bulk MoS_2 (190 mA h g^{-1}) can be enhanced using an exfoliated MoS_2/C composite (400 mA h g^{-1} even after 100 cycles) [94,95], A similar heterostructure or a composite approach might enhance the Na or K storage capacity of the present GeSe sheet even more. Table S1 provides a comparison of theoretical capacities among different 2D materials.

We compare the specific capacities of the bulk GeSe with those of 2D GeSe. Firstly, we checked the thermodynamic stability of metal atom insertion by calculating the average adsorption energy (E_{ave}). The E_{ave} s of Li, Na, and K are −0.85, −0.76, and −0.78 eV per alkali metal atom, respectively. The fully lithiated (sodiated and potassiated) bulk GeSe can hold only one Li (Na and K) atom per unit cell with chemical stoichiometries of $Li_{0.5}GeSe$. Therefore, the theoretical capacity of the bulk GeSe (~88.5 mA h g^{-1}) is much lower than the 2D GeSe. We also investigate the degree of bulk GeSe-volume expansion on full Li, Na, and K insertion. With Li insertion, the volume of the bulk GeSe is increased by 6.71%, whereas the volume expansions for the Na and K cases are 11.34% and 20.40%, respectively. These volume enlargements are quite small compared to those of Si, Ge, and Sn anodes. The expansion on lithium intercalation is even smaller than that of graphite (~12%) [96].

In all our DFT calculations, we used the DFT + D2 semiempirical correction of Grimme to include the van der Waals (vdW) interactions. Comparing our results with other semiempirical or fully nonlocal

correction schemes would be more comprehensive. However, we expect that the present results will not deviate much, as the DFT + D2 method is well known to describe the adsorption energy and diffusion of Li in graphite with good accuracy [41]. An organized comparison of adsorption and diffusion behaviors with different vdW correction schemes is left as a future work.

4. Conclusion

Using DFT calculations, we illustrate the prospective features of a 2D GeSe sheet for Na and K ion battery applications. The formation energy and phonon spectra of the GeSe sheet confirm the energetic and dynamic stabilities of this 2D material. Our calculation suggests that the GeSe sheet can be exfoliated from the bulk material. All the alkali metal atoms strongly adsorb to the GeSe sheet. Na (0.115 eV) and K (0.11 eV) atoms easily diffuse on the GeSe sheet, giving a rapid charge-discharge rate for NIB or KIB application. A substantial charge transfer from metal to GeSe modifies the semiconducting 2D GeSe to a metallic one, giving an enhanced electrical conductivity. A relatively high capacity for Na ($707\ mA\,h\,g^{-1}$) or K ($530\ mA\,h\,g^{-1}$) demonstrates that the 2D GeSe sheet can serve as an efficient anode material for a NIB or KIB. Among group-IV monochalcogenides, the 2D SiS is theoretically predicted to be best suited for LIB applications [21,35,49]. The current study further reveals that the 2D GeSe emerges as the most promising candidate for Na-ion and K-ion battery applications, having a better theoretical capacity and an energy density than the other members [21,92].

Notes

The authors declare no competing financial interest.

CRediT authorship contribution statement

Arindam Sannyal: Methodology, Software, Formal analysis, Data curation, Writing-original draft, Visualization. **Zhengqing Zhang: S**oftware, Visualization. **Xingfa Gao**: Conceptualization, Methodology, Formal analysis, Writing-review & editing. **Joonkyung Jang: C**onceptualization, Methodology, Formal analysis, Investigation, Resources, Writing-review & editing, Supervision, Project administration, Funding acquisition.

Acknowledgements

This study was supported by National Research Foundation Grants funded by the Korean Government (MSIP, NRF2014R1A4A1001690 and NRF-2018R1A2A2A05019776).

Data availability

The raw/processed data required to reproduce these findings cannot be shared at this time due to legal or ethical reasons.

Appendix A. Supplementary material

Supplementary data associated with this article can be found, in the online version, at https://doi.org/10.1016/j.commatsci.2018.08.002.

References

[1] J.M. Tarascon, Is lithium the new gold? Nat. Chem. 2 (2010) 510.
[2] J.-Y. Hwang, S.-T. Myung, Y.-K. Sun, Sodium-ion batteries: present and future, Chem. Soc. Rev. 46 (2017) 3529–3614.
[3] P.K. Nayak, L. Yang, W. Brehm, P. Adelhelm, From lithium-ion to sodium-ion batteries: advantages, challenges, and surprises, Angew. Chem. Int. Ed. 57 (2018) 102–120.
[4] X. Wu, D.P. Leonard, X. Ji, Emerging non-aqueous potassium-ion batteries: challenges and opportunities, Chem. Mater. 29 (2017) 5031–5042.
[5] J.C. Pramudita, D. Sehrawat, D. Goonetilleke, N. Sharma, An initial review of the status of electrode materials for potassium-ion batteries, Adv. Energy Mater. 7 (2017) 1602911.
[6] F. Li, Z. Zhou, Micro/nanostructured materials for sodium ion batteries and capacitors, Small 14 (2018) 1702961.
[7] X. Zhang, Z. Zhang, S. Yao, A. Chen, X. Zhao, Z. Zhou, An effective method to screen sodium-based layered materials for sodium ion batteries, npj Comput. Mater. 13 (2018) 1–6.
[8] K. Kubota, S. Komab, Review-practical issues and future perspective for Na-ion batteries, J. Electrochem. Soc. 162 (2015) A2538–A2550.
[9] N. Yabuuchi, K. Kubota, M. Dahbi, S. Komaba, Research development on sodium-ion batteries, Chem. Rev. 114 (2014) 11636–11682.
[10] L. Shi, T. Zhao, Recent advances in inorganic 2D materials and their applications in lithium and sodium batteries, J. Mater. Chem. A 5 (2017) 3735–3758.
[11] Q. Tang, Z. Zhou, P. Shen, Are MXenes promising anode materials for Li ion batteries? computational studies on electronic properties and Li storage capability of Ti_3C_2 and $Ti_3C_2X_2$ (X = F, OH) monolayer, J. Am. Chem. Soc. 134 (2012) 16909–16916.
[12] Y. Xie, Y. Dall'Agnese, M. Naguib, Y. Gogotsi, M.W. Barsoum, H.L. Zhuang, P.R.C. Kent, Prediction and characterization of MXene nanosheet anodes for non-lithium-ion batteries, ACS Nano 8 (2014) 9606–9615.
[13] E. Yang, H. Ji, Y. Jung, Two-dimensional transition metal dichalcogenide monolayers as promising sodium ion battery anodes, J. Phys. Chem. C 119 (2015) 26374–26380.
[14] R. Bhandavat, L. David, G. Singh, Synthesis of surface-functionalized WS_2 nanosheets and performance as Li-ion battery anodes, J. Phys. Chem. Lett. 3 (2012) 1523–1530.
[15] X. Zhang, Z. Yu, S.-S. Wang, S. Guan, H.Y. Yang, Y. Yao, S.A. Yang, Theoretical prediction of MoN_2 monolayer as a high capacity electrode material for metal ion batteries, J. Mater. Chem. A 4 (2016) 15224–15231.
[16] D. Rao, L. Zhang, Z. Meng, X. Zhang, Y. Wang, G. Qiao, X. Shen, H. Xia, J. Liu, R. Lu, Ultrahigh energy storage and ultrafast ion diffusion in borophene-based anodes for rechargeable metal ion batteries, J. Mater. Chem. A 5 (2017) 2328–2338.
[17] W. Li, Y. Yang, G. Zhang, Y.-W. Zhang, Ultrafast and directional diffusion of lithium in phosphorene for high-performance lithium-ion battery, Nano Lett. 15 (2015) 1691–1697.
[18] V.V. Kulish, O.I. Malyi, C. Perssoncd, P. Wu, Phosphorene as an anode material for Na-ion batteries: a first-principles study, Phys. Chem. Chem. Phys. 17 (2015) 13921–13928.
[19] X. Liu, Y. Wen, Z. Chen, B. Shan, R. Chen, A first-principles study of sodium adsorption and diffusion on phosphorene, Phys. Chem. Chem. Phys. 17 (2015) 16398–16404.
[20] W. Li, H. Li, Z. Lu, L. Gan, L. Ke, T. Zhai, H. Zhou, Layered phosphorus-like GeP_5: a promising anode candidate with high initial coulombic efficiency and large capacity for lithium ion batteries, Energy Environ. Sci. 8 (2015) 3629–3636.
[21] F. Li, Y. Qu, M. Zhao, Germanium sulfide nanosheet: a universal anode material for alkali metal ion batteries, J. Mater. Chem. A 4 (2016) 8905–8912.
[22] G. Wang, W.J. Slough, R. Pandey, S.P. Karna, Degradation of phosphorene in air: understanding at atomic level, 2D Mater. 3 (2016) 025011.
[23] A. Avsar, I.J. Vera-Marun, J.Y. Tan, K. Watanabe, T. Taniguchi, A.H.C. Neto, B. Ozyilmaz, Air-stable transport in graphene-contacted, fully encapsulated ultrathin black phosphorus-based field-effect transistors, ACS Nano 9 (2015) 4138–4145.
[24] T. Hu, J. Hong, Anisotropic effective mass, optical property, and enhanced band gap in BN/phosphorene/BN heterostructures, ACS Appl. Mater. Interfaces 7 (2015) 23489–23495.
[25] Y. Hu, S. Zhang, S. Sun, M. Xie, B. Cai, H. Zeng, GeSe monolayer semiconductor with tunable direct band gap and small carrier effective mass, Appl. Phys. Lett. 107 (2015) 122107.
[26] A.K. Singh, R.G. Hennig, Computational prediction of two-dimensional group-IV mono-chalcogenides, Appl. Phys. Lett. 105 (2014) 042103.
[27] L.C. Gomes, A. Carvalho, Phosphorene analogues: Isoelectronic two-dimensional group-IV monochalcogenides with orthorhombic structure, Phys. Rev. B 92 (2015) 085406.
[28] A. Shafique, Y.-H. Shin, Thermoelectric and phonon transport properties of two-dimensional IV–VI compounds, Sci. Rep. 7 (2017) 506.
[29] Y. Guo, S.Z.Y. Bai, J. Zhao, Oxidation resistance of monolayer group-IV monochalcogenides, ACS Appl. Mater. Interfaces 9 (2017) 12013–12020.
[30] S.C. Liu, Y. Mi, D.J. Xue, Y.X. Chen, C. He, X. Liu, J.S. Hu, L.J. Wan, Investigation of physical and electronic properties of GeSe for photovoltaic applications, Adv. Electron. Mater. 3 (2017) 1700141.
[31] P. Ramasamy, D. Kwak, D.H. Lim, H.S. Ra, J.S. Lee, Solution synthesis of GeS and GeSe nanosheets for high-sensitivity photodetectors, J. Mater. Chem. C 4 (2016) 479–485.
[32] D.D. Vaughn, R.J. Patel, M.A. Hickner, R.E. Schaak, Single-crystal colloidal nanosheets of GeS and GeSe, J. Am. Chem. Soc 132 (2010) 15170–15172.
[33] H.S. Im, Y.R. Lim, Y.J. Cho, J. Park, E.H. Cha, H.S. Kang, Germanium and tin selenide nanocrystals for high-capacity lithium ion batteries: comparative phase conversion of germanium and tin, J. Phys. Chem. C 118 (2014) 21884–21888.
[34] H. Kim, Y. Son, J. Lee, M. Lee, S. Park, J. Cho, H.C. Choi, Nanocomb architecture design using germanium selenide as high-performance lithium storage material, Chem. Mater. 28 (2016) 6146–6151.
[35] Y. Zhou, MX (M = Ge, Sn; X = S, Se) sheets: theoretical prediction of new promising electrode materials for Li ion batteries, J. Mater. Chem. A 4 (2016) 10906–10913.
[36] G. Kresse, J. Furthmüller, Efficient iterative schemes for ab initio total-energy

calculations using a plane-wave basis set, Phys. Rev. B: Condens. Matter Mater. Phys. 54 (1996) 11169–11186.
[37] G. Kresse, D. Joubert, From ultrasoft pseudopotentials to the projector augmented-wave method, Phys. Rev. B: Condens. Matter Mater. Phys. 59 (1999) 1758–1775.
[38] P.E. Blöchl, Projector augmented-wave method, Phys. Rev. B: Condens. Matter Mater. Phys. 50 (1994) 17953–17979.
[39] J.P. Perdew, K. Burke, M. Ernzerhof, Generalized gradient approximation made simple, Phys. Rev. Lett. 77 (1996) 3865–3868.
[40] S. Grimme, Semiempirical GGA-type density functional constructed with a long-range dispersion correction, J. Comput. Chem. 27 (2006) 1787–1799.
[41] P. Ganesh, J. Kim, C. Park, M. Yoon, F.A. Reboredo, P.R.C. Kent, Binding and diffusion of lithium in graphite: quantum Monte Carlo benchmarks and validation of van der Waals density functional methods, J. Chem. Theory Comput. 10 (2014) 5318–5323.
[42] A. Togo, I. Tanaka, First principles phonon calculations in materials science, Scr. Mater. 108 (2015) 1–5.
[43] H.J. Monkhorst, J.D. Pack, Special points for Brillonin-zone integrations, Phys. Rev. B: Condens. Matter Mater. Phys. 13 (1976) 5188–5192.
[44] W. Tang, E. Sanville, G. Henkelman, A grid-based Bader analysis algorithm without lattice bias, J. Phys. Condens. Matter 21 (2009) 084204.
[45] E. Sanville, S.D. Kenny, R. Smith, G. Henkelman, Improved grid-based algorithm for bader charge allocation, J. Comput. Chem. 28 (2007) 899.
[46] G. Henkelman, A. Arnaldsson, H. Jonsson, A fast and robust algorithm for Bader decomposition of charge density, Comput. Mater. Sci. 36 (2006) 354–360.
[47] G. Henkelman, B.P. Uberuaga, H. Jansson, A climbing image nudged elastic band method for finding saddle points and minimum energy paths, J. Chem. Phys. 113 (2000).
[48] G. Henkelman, H. Jansson, Improved tangent estimate in the nudged elastic band method for finding minimum energy paths and saddle points, J. Chem. Phys. 113 (2000) 9978–9985.
[49] S. Karmakar, C. Chowdhury, A. Datta, Two-dimensional group IV monochalcogenides: anode materials for Li-ion batteries, J. Phys. Chem. C 120 (2016) 14522–14530.
[50] C. Chowdhury, S. Karmakar, A. Datta, Capping black phosphorene by h-BN enhances performances in anodes for Li and Na ion batteries, ACS Energy Lett. 1 (2016) 253–259.
[51] Y. Zhou, MX (M = Ge, Sn; X = S, Se), sheets: theoretical prediction of new promising electrode materials for Li ion batteries, J. Mater. Chem. A (2016) 10906.
[52] M.K. Aydinol, A.F. Kohan, G. Ceder, K. Cho, J. Joannopoulos, Ab initio study of lithium intercalation in metal oxides and metal dichalcogenides, Phys. Rev. B: Condens. Matter Mater. Phys. 56 (1997) 1354–1365.
[53] A. Jain, G. Hautier, S.P. Ong, C.J. Moore, C.C. Fischer, K.A. Persson, G. Ceder, Formation Enthalpies by Mixing GGA and GGA + U Calculations, Phys. Rev. B: Condens. Matter 84 (2011) 045115.
[54] X. Gonze, C.Y. Lee, Dynamical matrices, born effective charges, dielectric permittivity tensors, and interatomic force constants from density-functional perturbation theory, Phys. Rev. B: Condens. Matter Mater. Phys. 55 (1997) 10355–10368.
[55] B.D. Kong, S. Paul, M.B. Nardelli, K.W. Kim, First-principles analysis of lattice thermal conductivity in monolayer and bilayer graphene, Phys. Rev. B: Condens. Matter 80 (2009) 033406.
[56] G. Qin, Q.-B. Yan, Z. Qin, S.-Y. Yue, M. Hu, G. Su, Anisotropic intrinsic lattice thermal conductivity of phosphorene from first principles, Phys. Chem. Chem. Phys. 17 (2015) 4854–4858.
[57] B. Peng, H. Zhang, H. Shao, Y. Xu, X. Zhang, H. Zhu, Low lattice thermal conductivity of stanene, Sci. Rep. 6 (2016) 20225.
[58] F. Wu, C. Huang, H. Wu, C. Lee, K. Deng, E. Kan, P. Jena, Atomically thin transition-metal dinitrides: high-temperature ferromagnetism and half-metallicity, Nano Lett. 15 (2015) 8277–8281.
[59] J.H. Jung, C.-H. Park, J. Ihm, A rigorous method of calculating exfoliation energies from first principles, Nano Lett. 18 (2018) 2759–2765.
[60] B. Radisavljevic, A. Radenovic, J. Brivio, V. Giacometti, A. Kis, Single-layer MoS_2 transistors, Nat. Nanotechnol. 6 (2011) 147–150.
[61] Z. Yu, Y. Pan, Y. Shen, Z. Wang, Z. Ong, T. Xu, R. Xin, L. Pan, B. Wang, L. Sun, J. Wang, G. Zhang, Y. Zhang, Y. Shi, X. Wang, Towards intrinsic charge transport in monolayer molybdenum disulfide by defect and interface engineering, Nat. Commun. 5 (2014) 5290.
[62] V. Nicolosi, M. Chhowalla, M.G. Kanatzidis, M.S. Strano, J.N. Coleman, Liquid exfoliation of layered materials, Science 340 (2013) 1226419.
[63] J.N. Coleman, Two-dimensional nanosheets produced by liquid exfoliation of layered materials, Science 331 (2011) 568–571.
[64] E. Lee, K.A. Persson, Li absorption and intercalation in single layer graphene and few layer graphene by first principles, Nano Lett. 12 (2012) 4624–4628.
[65] X. Fan, W.T. Zheng, J.-L. Kuo, D.J. Singh, Adsorption of single Li and the formation of small Li clusters on graphene for the anode of lithium-ion batteries, ACS Appl. Mater. Interfaces 5 (2013) 7793–7797.
[66] T. Hu, J. Hong, First-principles study of metal adatom adsorption on black phosphorene, J. Phys. Chem. C 119 (2015) 8199–8207.
[67] H. Sahin, F.M. Peeters, Adsorption of alkali, alkaline-earth, and 3d transition metal atoms on silicene, Phys. Rev. B: Condens. Matter Mater. Phys. 87 (2013) 085423.
[68] F.W. Averill, Calculation of the cohesive energies and bulk properties of the alkali metals, Phys. Rev. B 6 (1972) 3637–3642.
[69] P. Bhauriyal, A. Mahata, B. Pathak, Graphene-like carbon − nitride monolayer: a potential anode material for Na- and K-ion batteries, J. Phys. Chem. C 122 (2018) 2481–2489.
[70] S. Zhang, S. Liu, S. Huang, B. Cai, M. Xie, L. Qu, Y. Zou, Z. Hu, X. Yu, H. Zeng, Structural and electronic properties of atomically thin germanium selenide polymorphs, Sci. China Mater. 58 (2015) 929–935.
[71] Q. Sun, Y. Dai, Y. Ma, T. Jing, W. Wei, B. Huang, Ab initio prediction and characterization of Mo_2C monolayer as anodes for lithium-ion and sodium-ion batteries, J. Phys. Chem. Lett. 7 (2016) 937–943.
[72] D. Cakr, C. Sevik, O. Gulseren, F.M. Peeters, Mo_2C as a high capacity anode material: a first principles study, J. Mater. Chem. A 4 (2016) 6029–6035.
[73] C. Uthaisar, V. Barone, Edge effects on the characteristics of Li diffusion in graphene, Nano Lett. 10 (2010) 2838–2842.
[74] V.V. Kulish, O.I. Malyi, M.F. Ng, P. Wu, Z. Chen, Enhanced Li adsorption and diffusion in silicon nanosheets based on first principles calculations, RSC Adv. 3 (2013) 4231–4236.
[75] W. Wan, Q. Zhang, Y. Cui, E. Wang, First principles study of lithium insertion in bulk silicon, J. Phys. Condens. Matter 22 (2010) 415501.
[76] C. Chou, H. Kim, G.S. Hwang, A comparative first-principles study of the structure, energetics, and properties of Li-M (M = Si, Ge, Sn) alloys, J. Phys. Chem. C 115 (2011) 20018–20026.
[77] M.V. Koudriachova, N.M. Harrison, S.W. Leeuw, Effect of diffusion on lithium intercalation in titanium dioxide, Phys. Rev. Lett. 86 (2001) 1275–1278.
[78] M. Wagemaker, R.v.d. Krol, A.P. Kentgens, A.A.V. Well, F.M. Mulder, Two phase morphology limits lithium diffusion in TiO_2 (anatase): a ^{7}Li MAS NMR study, J. Am. Chem. Soc. 123 (2001) 11454–11461.
[79] A. Urban, D.-H. Seo, G. Ceder, Computational understanding of Li-ion batteries, npj Comput. Mater. 2 (2016) 16002.
[80] L. Shi, T. Zhao, A. Xu, J. Xu, Ab initio prediction of borophene as an extraordinary anode material exhibiting ultrafast directional sodium diffusion for sodium-based batteries, Sci. Bull. 61 (2016) 1138–1144.
[81] Z. Yang, R. Li, Z. Deng, A deep study of the protection of Lithium Cobalt Oxide with polymer surface modifcation at 4.5V high voltage, Sci. Rep. 8 (2018) 863.
[82] J. Hu, B. Xu, C. Ouyang, Y. Zhang, S.A. Yang, Investigations on Nb_2C monolayer as promising anode material for Li or non-Li ion batteries from first-principles calculations, RSC Adv. 6 (2016) 27467–27474.
[83] J. Hu, B. Xu, S.A. Yang, S. Guan, C. Ouyang, Y. Yao, 2D electrides as promising anode materials for Na-ion batteries from first-principles study, ACS Appl. Mater. Interfaces 7 (2015) 24016–24022.
[84] S.P. Ong, W.D. Richards, A. Jain, G. Hautier, M. Kocher, S. Cholia, D. Gunter, V.L. Chevrier, K.A. Persson, G. Ceder, Python materials genomics (pymatgen): a robust, open-source python library for materials analysis, Comput. Mater. Sci. 68 (2013) 314–319.
[85] X. Lv, W. Wei, Q. Sun, L. Yu, B. Huang, Y. Dai, Sc_2C as a promising anode material with high mobility and capacity: a first-principles study, ChemPhysChem 18 (2017) 1627–1634.
[86] R.P. Joshi, B. Ozdemir, V. Barone, J.E. Peralta, Hexagonal BC_3: a robust electrode material for Li, Na, and K ion batteries, J. Phys. Chem. Lett. 6 (2015) 2728–2732.
[87] C.M. Julien, A. Mauger, K. Zaghib, H. Groult, Comparative issues of cathode materials for Li-ion batteries, Inorganics 2 (2014) 132–154.
[88] J.R. Dahn, Phase diagram of Li_xC_6, Phys. Rev. B: Condens. Matter Mater. Phys. 44 (1991) 9170–9177.
[89] Z. Yang, D. Choi, S. Kerisit, K.M. Rosso, D. Wang, J. Zhang, G. Graff, J. Liu, Nanostructures and lithium electrochemical reactivity of lithium titanites and titanium oxides: a review, J. Power Sour. 192 (2009) 588–598.
[90] J. Su, Y. Pei, Z. Yang, X. Wang, Ab initio study of graphene-like monolayer molybdenum disulfide as a promising anode material for rechargeable sodium ion batteries, RSC Adv. 4 (2014) 43183–43188.
[91] D.B. Putungan, S.-H. Lin, J.-L. Kuo, Metallic VS_2 monolayer polytypes as potential sodium-ion battery anode via ab initio random structure searching, ACS Appl. Mater. Interfaces 8 (2016) 18754–18762.
[92] H. Jiang, T. Zhao, Y. Ren, R. Zhang, M. Wu, Ab initio prediction and characterization of phosphorene-like SiS and SiSe as anode materials for sodium-ion batteries, Sci. Bull. 62 (2017) 572–578.
[93] K. Nobuhara, H. Nakayama, M. Nose, S. Nakanishi, H. Iba, First-principles study of alkali metal-graphite intercalation compounds, J. Power Sour. 243 (2013) 585–587.
[94] J. Park, J.S. Kim, J.W. Park, T.H. Nam, K.W. Kim, J.H. Ahn, G. Wang, H.J. Ahn, Discharge mechanism of MoS_2 for sodium ion battery: electrochemical measurements and characterization, Electrochim. Acta 92 (2013) 427–432.
[95] Y. Wang, K.H. Seng, S. Chou, Reversible sodium storage via conversion reaction of a MoS_2–C composite, Chem. Commun. 50 (2014) 10730–10733.
[96] W. Li, X. Sun, Y. Yu, Si Ge, Sn-based anode materials for lithium-ion batteries: from structure design to electrochemical performance, Small Methods 1 (2017).